Multimode interference: Highly regular pattern formation in quantum wave-packet evolution

A. E. Kaplan,[1] I. Marzoli,[2,*] W. E. Lamb, Jr.,[3] and W. P. Schleich[2]
[1]*Electrical and Computer Engineering Department, The Johns Hopkins University, Baltimore, Maryland 21218*
[2]*Abteilung für Quantenphysik, University of Ulm, D-89069 Ulm, Germany*
[3]*Optical Sciences Center, University of Arizona, Tucson, Arizona 85721*
(Received 19 July 1999; published 9 February 2000)

Highly regular spatiotemporal or multidimensional patterns in the quantum mechanical probability or classical field intensity distributions can appear due to pair interference between individual eigenmodes of the system, thus forming the so-called intermode traces. These patterns are strongly pronounced in any anharmonic potential, provided that the traces are multidegenerate; they may occur in many areas of wave physics.

PACS number(s): 03.65.Bz, 03.75.−b, 03.75.Dg, 41.20.Jb

I. INTRODUCTION

The controlled preparation and measurement of wave packets has recently emerged as an extremely active field of research. Examples include wave packets in atoms [1], optical lattices [2], ion traps [3], molecules [4], and semiconductor quantum wells [5], to name a few. One of the major points of interest is the spatiotemporal evolution of wave packets in such systems. Since most of the experiments engage a broad-spectrum excitation of the eigenmodes of the system, large-scale interference becomes a leading factor. It gives rise to well-ordered long-range regularities such as quantum revivals [6], interference patterns in the atomic double-slit experiment [7(a)], diffraction effects in atom optics [7(b)] and so called δ ionization [8]. In this paper, we show that these packets may also serve as a testing ground for another class of interference effects that have recently gained intense interest [7–15]: the formation of highly regular spatiotemporal or multidimensional patterns in the quantum mechanical probability, $|\psi|^2$, or classical electromagnetic field intensity, $|\mathcal{E}|^2$.

The patterns have been discovered in the probability density $|\psi(x,t)|^2$ of a particle confined to an infinitely deep square well, by performing numerical simulations of the evolution of a Gaussian wave packet [9], an initially homogeneous wave function [10(a)] or well localized wave packets [11], a Bose-Einstein condensate [12], and an angular wave packet [13]. In all cases, the probability distribution is characterized by a regular net of *canals*, minima of probability, and *ridges*, maxima of probability, which run along straight lines in space-time (x,t).

Similar patterns also arise in the near field of a diffraction grating illuminated with light [10(a)] as well as in matter waves in atom optics [7(b)]. Indeed, the paraxial approximation allows for a space-time analogy between quantum mechanics and electrodynamics. The space-time probability distribution $|\psi(x,t)|^2$ is mapped onto the field intensity $|\mathcal{E}(x,z)|^2$, where z is the propagation direction. For multidimensional problems, x is replaced by a radial vector $\vec{r}$ in the transverse cross section. In the simplest case of the square well (or plane geometry of EM-diffraction grating) this phenomenon reveals a new aspect of the so-called Talbot effect [14], which traditionally concerns only patterns in planes at *fixed* time t or distance z, i.e., ''slices'' of the distribution, instead of the patterns in the ''full propagation'' space (x,t) or (x,z).

The common feature of these systems is a broad-spectrum excitation: e.g., in the quantum case, the rich patterns appear only when many states are populated. So far the theory of these patterns has relied on the specific choice of the initial conditions and on the square well (or diffraction grating structure), with no simple physical explanation suggested. In our recent work [15] we observed a similar ''quantum carpet'' in both the square well and a smooth potential and offered an idea of a universal explanation for this phenomenon. The key mechanisms have been identified [15] as pair multiinterference between the eigenmodes of the system and the degeneracy of this interference.

Pair interference between the eigenmodes of the system, the underlying building blocks of carpet patterns, gives rise to the so called ''intermode traces,'' the lines of constant phase of interference terms. The phenomenon is strongly pronounced for degenerate (or nearly degenerate) traces, whereby many nonvanishing individual traces are superimposed to produce distinct patterns. Our theory describes analytically the major features of the quantum carpet. It not only explains the straight-line patterns observed in a square quantum box (or in the Talbot effect), but also predicts that distinct ''curved'' patterns can appear in anharmonic potentials, more pertinent to quantum mechanics. In this paper, we verify this by comparing the numerically generated patterns for these potentials with the results of our analytical calculations.

Most of our analytical results for the general case of anharmonic potentials rely on the WKB approximation. Therefore, in order to study the onset of the intermode traces, we discuss in detail the dependence of these patterns on the initial momentum of the wave packet (or the amplitude of the δ-kick producing this momentum). For this purpose, we show not only the numerically generated patterns for various excitations beginning from zero and follow the intermode trace formation, but also display the populations of all the quantum levels engaged. In order to address more realistic and universal situations, we start from the most natural initial

*Permanent address: Dipartimento di Matematica e Fisica and INFM, Università di Camerino, 62032 Camerino (MC), Italy.

state of the system, that is *a ground state* and then add a momentum to it, instead of assuming a (relatively artificial) tight initial packet (as was assumed in most of work [7–15]), which has to engage already many excited eigenstates even before the momentum is added. We emphasize that some of our important results are that even for these ''smoothed-out'' initial packets in anharmonic oscillators, the intermode traces begin transpiring even at relatively low excitations, with just a few low lying quantum levels involved.

II. INTERMODE TRACES IN 1D POTENTIALS

The wave function $\psi(\vec{r},t)$ of a quantum particle with mass m_e moving in a potential $U(\vec{r})$ is governed by the Schrödinger equation,

$$i\hbar\,\partial\psi/\partial t-[\hat{T}+U(\vec{r})]\psi=0. \tag{1}$$

Here $\hbar$ is Planck constant, and $\hat{T}\equiv-(\hbar^2/2m_e)\nabla^2$ is the operator of the kinetic energy.

We note that Maxwell equations of classical electrodynamics can also be approximated by the same equation under the assumption of small diffraction and fixed polarization. In the resulting scalar equation, ψ is replaced by the field amplitude $\mathcal{E}$, U by the dielectric constant ϵ, ∇^2 by the ''transverse'' Laplacian, time t by the longitudinal coordinate z of propagation, and $\hbar$ by the wavelength λ; the limits $\hbar\to 0$ and $\lambda\to 0$ correspond to classical mechanics and ray optics, respectively. This so-called paraxial approximation is valid for many problems related to the optics of well collimated fields, e.g., in lasers and some microwave devices.

To develop the basic theory of intermode traces, we consider here only one-dimensional (1D) problems, that is problems which involve either spatiotemporal patterns in quantum mechanics with one coordinate and a time variable, or spatial patterns in optics with one transverse and one longitudinal variable. A similar phenomenon in higher dimensions will be considered by us elsewhere.

To study the time evolution of a particle moving in a 1D binding potential $U(x)$, we write the full wave function as

$$\psi(x,t)=\sum_{n=1}^{\infty} a_n\psi_n(x,t), \tag{2}$$

where

$$\psi_n(x,t)=\tilde{\psi}_n(x)\exp(-E_nt/\hbar) \tag{3}$$

are energy eigenfunctions of energies E_n, with their amplitudes $a_n=$const determined by the initial conditions, and $\tilde{\psi}_n(x)$ is the spatially dependent component of ψ_n. To bring out the spatiotemporal patterns of the probability density, $|\psi|^2$, we represent it is as the sum of ''elementary'' intermode terms, μ_{nm}:

$$|\psi(x,t)|^2=\sum_{n,m=1}^{\infty}\mu_{nm}(x,t), \tag{4}$$

where

$$\mu_{nm}(x,t)\equiv(1/2)\sigma_{nm}\psi_n(x,t)\psi_m^*(x,t)+\text{c.c.}, \tag{5}$$

is an intermode term with $\sigma_{nm}\equiv a_na_m^*=$const being the density matrix element. We now break the density (4) down into time-independent term, $I_0(x)=\Sigma_n\mu_{nn}$ with all the diagonal components, $\mu_{nn}=\sigma_{nn}|\psi_n|^2$, where σ_{nn} are the populations of the respective quantum levels, and the ''interference'' term, which is the sum over all the nondiagonal components, $\mu_{n\neq m}$; its average over long time vanishes. The latter, interference term with the sum of elementary intermode terms (5) helps us to keep a ''global'' view of the spatiotemporal evolution of $|\psi|^2$.

Insofar as the quantum carpet engages many excited states, we are dealing with a situation best handled by the WKB method [16]. We therefore represent the eigenwave functions (3) as a superposition of ''WKB'' functions

$$\psi_n^{(\mathrm{WKB})}(x,t)\approx f_n(x)\exp\left[\pm i\int k_n(x)dx-iE_nt/\hbar\right]. \tag{6}$$

Here both the preexponential factor $f_n(x)$ and the momentum

$$\hbar k_n(x)=\sqrt{2m_e[E_n-U(x)]} \tag{7}$$

are assumed to vary slowly compared to $\exp[\pm i\int k_n(x)dx]$.

The eigenenergies E_n are evaluated using the Bohr-Sommerfeld condition

$$\int_{x_l}^{x_r}k_n\,dx=n\pi,$$

where $x_{l,r}$ are the left and right turning points of a classical trajectory, respectively. They are determined by the condition $E_n=U(x)$. For example, if $U\propto|x|^w$ with $w>-2$, one has [17]

$$E_n\propto n^{2w/(2+w)}. \tag{8}$$

The rapidly oscillating functions in an elementary interference term, $\mu_{n\neq m}$, are then $\exp(\pm i\zeta_{nm})$, where

$$\zeta_{nm}(x,t)=\int[k_n(x)\pm k_m(x)]dx\pm(E_n-E_m)t/\hbar. \tag{9}$$

Note that two pairs of signs, ''$\pm$,'' in front of both momentum and energy, are *independent* of each other, so that in Eq. (9) we have *four* different phases $\zeta_{nm}(x,t)$. We now look at the lines of constant phase, $\zeta_{nm}(x,t)=$const. They are space-time trajectories which define the traces. We find their velocities as

$$v_{nm}(x)=\left(\frac{dx}{dt}\right)_{nm}=\frac{(\Delta\omega)_{nm}}{(\Delta k)_{nm}}, \tag{10}$$

where

$$(\Delta\omega)_{nm}\equiv(E_n-E_m)/\hbar,\quad (\Delta k)_{nm}\equiv\pm[k_n(x)\pm k_m(x)]. \tag{11}$$

With the help of Eq. (9) we obtain for v_{nm}

$$\nu_{nm}(x) \equiv \pm \frac{\omega_n - \omega_m}{k_n \pm k_m} \approx \pm \frac{(E_n - E_m)\sqrt{2m_e}}{\sqrt{E_n - U(x)} \pm \sqrt{E_m - U(x)}}, \tag{12}$$

where $\omega_n \equiv E_n/\hbar$. Note again that we have here *four* different velocities.

The trajectory is then

$$t = \int_{x_I}^{x} \nu_{nm}^{-1}\, dx, \tag{13}$$

where x_1 is the turning point for the lower energy E_n and E_m. For every pair of quantum numbers n and m we find *four* traces, with all the possible combination of signs in Eq. (12). The density matrix elements, σ_{nm}, determine the ''weight'' of the (n,m) trace via $|\sigma_{nm}|$, and its positioning via the phase ϕ_{nm}, defined by $\exp(i\phi_{nm}) = \sigma_{nm}/|\sigma_{nm}|$.

When $\Delta\omega, \Delta k$ are large, the velocity ν_{nm} approaches the phase velocity, and describes strictly quantum features of the motion. In contrast, when $\Delta\omega, \Delta k$ are small, ν_{nm} is reminiscent of a group velocity corresponding to a classical motion of a particle. Indeed, an initially almost classical motion is described by a compact group of eigenmodes near some high quantum number N, with a number ΔN of these modes satisfying the condition $1 \ll \Delta N \ll N$. This excitation results in a strong *clustering of traces in two groups*. The one with

$$|(\Delta\omega)_{n,m}| \ll \omega_N, \quad \textit{and} \quad (\Delta k)_{n,m} \ll |k_N|, \tag{14}$$

is essentially a *classical* trajectory, since in such a case

$$\frac{(\Delta\omega)_{n,m}}{(\Delta k)_{n,m}} \approx \frac{d\omega}{dk} \equiv \nu_{\rm gr}, \tag{15}$$

where $\nu_{\rm gr}$ is a group velocity. It coincides with the classical velocity, since the intermode trace equation obtained from Eq. (12) as

$$\frac{dx}{dt} = \sqrt{2[E_N - U(x)]/m_e}, \tag{16}$$

describes classical motion of a particle with energy E_N in a potential $U(x)$.

One can see now that the other group of traces, with

$$\nu_{nm} \ll \nu_{\rm gr}, \quad \textit{and} \quad |k_n \pm k_m| \approx |2k_N|, \tag{17}$$

reflects the *quantum* behavior. Remarkably, the WKB approximation developed basically as a tool to describe quasiclassical motion, can also serve to describe highly quantum objects like the ''quantum'' group of intermode traces. The full set of velocities ν_{nm} (12), ranging from group velocity to phase velocity at the extremes, provides a greatly useful tool in the understanding of quantum system.

III. SQUARE WELL POTENTIAL WITH INFINITE WALLS

As an illustration, we consider first the simplest potential, the square well potential with infinite walls. In the EM analogy, this corresponds to an EM wave in a waveguide with ideal metallic walls. In this case, the WKB results become *exact*, so that for a box of width L the ground-state frequency and wave number are

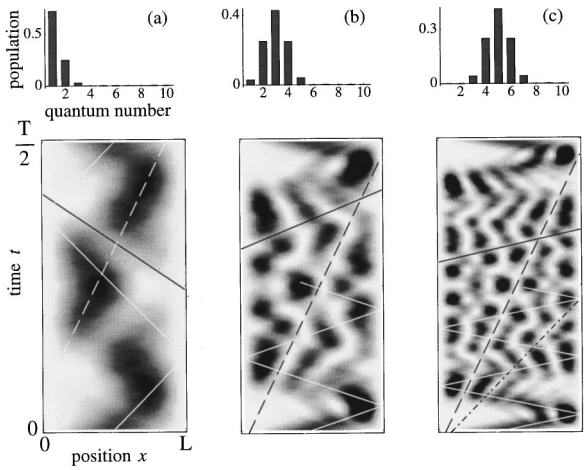

FIG. 1. A wave packet formed by a ground state wave function moving with different initial momenta $\overline{p}$ in a square well creates patterns in the probability distribution $|\psi|^2$ in space-time (x,t). The dark blobs correspond to the maxima of $|\psi|^2$, the light areas to its minima. The examples of intermode traces: solid white curves—classical trajectories, solid black curves—''near-classical'' traces, and broken curves—''quantum'' traces (see the text). Upper diagrams show population σ_{nn} vs the quantum state number, n. (a) $\overline{p}=1$; (b) $\overline{p}=3$; (c) $\overline{p}=5$.

$$\omega_1 = \frac{\hbar\pi^2}{2m_e L^2}, \quad \textit{and} \quad k_1 = \frac{\pi}{L}, \tag{18}$$

respectively. The eigenfrequencies, eigenenergies, and eigenwave numbers then are respectively

$$\omega_n = n^2\omega_1, \quad E_n = \hbar\omega_n, \quad \textit{and} \quad k_n = nk_1; \quad n = 1,2,3,\ldots. \tag{19}$$

For the box problem, the expression for the trace velocity (12) becomes *exact*, and reads

$$\nu_{nm} = \pm M \cdot \nu_{\square}, \quad M = m \pm n; \tag{20}$$

where M is the normalized velocity, and

$$\nu_{\square} = c\,\frac{\lambda_C}{4L} \ll c, \tag{21}$$

is a characteristic velocity of a box, and $\lambda_C \equiv 2\pi\hbar/cm_e = 2.4\times10^{-10}$ cm is the Compton wavelength.

Since M in Eq. (20) is an integer, a trace with a certain M is attributed to *all* the couples of modes n and m whose sum or difference is M. If the number of the states involved is sufficiently large, this trace degeneracy creates multiple superimposed traces. They in turn give rise to the distinct straight canals in Fig. 1.

In Fig. 1 we show some of the traces predicted by Eq. (20). Here we assume that the initial wave packet is the

ground state wave function, i.e., $\psi_1(x) \propto \sin(\pi x/L)$. The system is hit by a δ-pulse delivering a momentum $\overline{p}$, which we normalize to the ground state momentum $p_1 = \hbar k_1$. We show the time evolution of $|\psi|^2$ from $t=0$ to $T/2$, with $T \equiv 2\pi/\omega_1$ being the revival time, after which the initial wave packet reshapes itself [6].

The population distribution, σ_{nn}, is shown in the upper diagrams of Fig. 1. When the excitation is relatively low, $\overline{p} = 1$, Fig. 1(a), only two eigenstates are involved. The classical trajectory (white solid line), bouncing between the walls, does not fit any pattern yet even though it has the same velocity as some of them. There are only two traces, not well fitting either: a ''near-classical'' trace (black solid line) created by selecting $k_n - k_m$ in Eq. (12) [or normalized velocity $M = n + m$ in Eq. (20)] with $(n,m) = (1,2)$, and a ''quantum'' trace, white dashed line, corresponding to $k_n + k_m$ in Eq. (12) [or $M = n - m$ in Eq. (20)].

For stronger excitation, $\overline{p} = 3$, Fig. 1(b) there are several traces with the same velocities fitting the straight patterns which emerge now more clearly. The black solid line for a near-classical trace is twofold degenerate since pairs (2,3) and (1,4) lead to the same $M = n + m = 5$. The quantum trace (broken line) is highly degenerate, being produced by pairs (1,2), (2,3), (3,4) and (4,5) with $M = |n - m| = 1$.

A more developed quantum carpet is seen in Fig. 1(c) for $\overline{p} = 5$. Beside the classical trajectory, white solid line, and a near-classical trace (black solid line) for $M = n + m = 9$ [with the pairs (3,6) and (4,5)], one can see two examples of quantum intermode traces: for $|n - m| = 1$ (dashed line), generated by pairs (3,4), (4,5), (5,6) and (6,7), and for $|n - m| = 2$ (dash-dotted line) with pairs (3,5), (4,6) and (5,7).

IV. AN ARBITRARY ANHARMONIC POTENTIAL

It is obvious that the phenomenon is not restricted to the square well; it should occur for other potentials. Distinct patterns near *the classical trajectory* are better pronounced for strongly anharmonic potentials with ''hard walls,'' the extreme example of which is a box, and less for ''soft'' potentials, e.g., $U \propto |x|^w$ with $w \leqslant 2$, including the harmonic potential, $w = 2$. This is explained by a high trace degeneracy in a box, whereby many individual traces with the *same* velocity bundle together to form the patterns; the soft potentials, on the other hand, create less degenerate traces. To illustrate this, we note from the definition of the trace velocity (12) that the peak velocity, i.e., the velocity at $U(x) = 0$, is

$$(\nu_{nm})_{\rm pk} \approx \pm(\sqrt{E_n} \pm \sqrt{E_m})/\sqrt{2m_e}. \tag{22}$$

Hence, if $E_n \propto n^2$, as in a box, then $(\nu_{nm})_{\rm pk} \propto n \pm m$, Eq. (20), and there are many intermode trace pairs with n and m producing the same $\nu_{\rm pk}$.

On the other hand, for the harmonic potential, $w = 2$, with $E_n \propto n$ for large n, the only quantum numbers resulting in *exact* degeneracy of $(\nu_{nm})_{\rm pk}$, are $n,m = 1,4,9,16$, etc. However, by preparing the initial wave function out of these states alone (to be addressed by us elsewhere), one can produce a distinct quantum carpet.

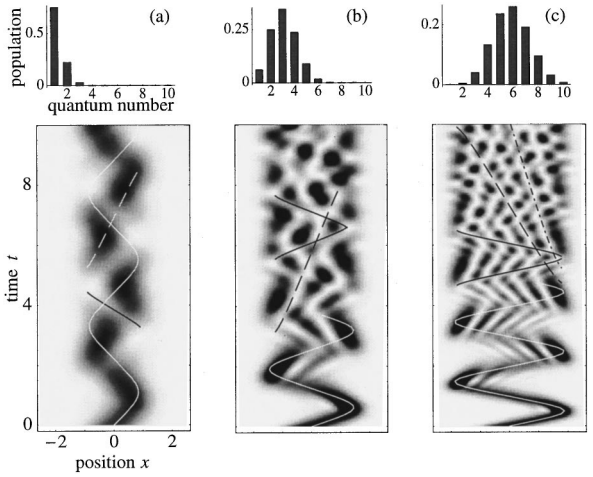

FIG. 2. Same as in Fig. 1 for a potential $U(\mathbf{x}) \propto x^4$.

We look now into the set of velocities $\nu_{nm}(x)$, where both n,m are *near* some fixed integer $N \gg 1$, with

$$n = N + \Delta n, \quad m = N + \Delta m, \quad \textit{and} \quad |\Delta n \pm \Delta m| \ll N.$$

Then, for the potential $U \propto |x|^w$, where w is now an arbitrary number, we have

$$\nu_{nm}(x) \approx \nu_{\rm gr}(E_N, x)\left[1 + \frac{(\Delta n + \Delta m)(w/2)}{N(2+w)} \frac{E_N}{\Delta E_N(x)} - \frac{(\Delta n^2 + \Delta m^2)(w/4)}{N^2(2+w)^2} \frac{E_N}{\Delta E_N(x)} \times \left(2 + \frac{w \cdot U(x)}{\Delta E_N(x)}\right) + \cdots\right], \tag{23}$$

where $\Delta E_N(x) = E_N - U(x)$.

Without the term with $\Delta n^2 + \Delta m^2$ in Eq. (23), all the intermode traces with, e.g., $\Delta n + \Delta m = 0$ would be degenerate. Comparing this term with the previous one in Eq. (23) at $|\Delta n + \Delta m| = 1$, we find the number of eigenmodes $\Delta N_d \equiv |\Delta n - \Delta m|_{\rm max}$, forming a group of nearly-degenerate intermode traces around a fixed state number $N \gg 1$ as [15]

$$\Delta N_d \sim \sqrt{\frac{N(2+w)}{2 + wU(x)/(E_N - U(x))}}. \tag{24}$$

Near the point $U(x) = 0$, the ratio $\Delta N_d/\sqrt{N}$ increases as w increases; for a box, we find $w = \infty$. This ratio also decreases in the area $E_N/2 < U(x) < E_N$ (which is very narrow for hard potentials), especially near turning points, $U(x) \to E_N$.

Let us discuss now a potential which represents an intermediate case between the square box and harmonic potential. Figure 2 depicts the quantum carpets for the anharmonic potential

$$U = Ax^4, \tag{25}$$

in which the initial wave packet is again a ground-state wave function hit by a δ-pulse delivering momentum $\overline{p}$ [18]. Here

we have introduced the system $m_e=\hbar=A=1$, that is we have scaled x, t, and p by the factors

$$x_s\equiv(\hbar^2/m_eA)^{1/6},\quad t_s\equiv(m_e^2/\hbar A)^{1/3},\quad \textit{and}\quad p_s\equiv m_e x_s/t_s, \tag{26}$$

respectively.

Figure 2(a) depicts a case of low excitation, $\bar{p}=1$, with only two states excited. Here, the classical trajectory (white solid line) does not produce a good fit yet while canals fit approximately to classical traces (black solid line), and ridges—to quantum traces (white dashed line) with $(m,n)=(1,2)$ in both cases.

We now turn to the case of higher excitation, $\bar{p}=3$, Fig. 2(b), with an almost classical distribution of state populations, σ_{nn}. Here the carpet is well pronounced. The classical trajectory fits snugly into maxima of $|\psi|^2$. Moreover, now the near-classical trace (black solid line) with pair $(m,n)=(2,3)$, fits very well the canal patterns. The quantum trace (dashed line) for the same pair also fits the respective patterns.

Finally, when $\bar{p}=5$, Fig. 2(c), one sees a pronounced classical motion for the first couple of cycles which then turns into a richly developed carpet well described by intermode traces. The dark solid lines are near-classical traces produced by the pair $(n,m)=(5,6)$, while broken lines denote a few examples of quantum traces: the dash-dotted one is created by the same pair, whereas the dashed one by (5,7).

V. IMPLICATIONS AND RELATIONS TO OTHER FIELDS

To excite many atomic eigenstates using a *ground* state as an initial wave packet, instead of Rydberg states, one needs to shake up the system by a strong δ-like EM pulse shorter than a cycle of any eigenfrequency; potential avenues to generate these pulses are multicascade stimulated Raman scattering [18(a)], molecule modulation [18(b)], subfemtosecond field solitons [18(c),18(d)] and very high harmonic generation [18(e)]. However, in solid-state quantum wells [5] subpicosecond half-cycle pulses can achieve the goal, while in atom optics of ion traps [3], with the motional frequency being in radiodomain, even a *nano*-second laser pulse can serve as a δ kick.

Insofar as the EM wave equation in paraxial approximation is isomorphous to the Schrödinger equation, the intermode traces can readily be found in optics and electrodynamics, with waveguides, resonators and spatially- or time-periodical structures providing a natural playground for EM mode interference. For example, the modes of a sufficiently wide, $L\gg\lambda$, wave guide with ideally conducting walls (as well as the field scattered by a diffraction grating in the Talbot effect) have the same patterns as those of the square well, Eq. (20). The modes of a regular fiber waveguide produce patterns similar to those of the box of finite width, while modes of a fiber waveguide with smoothly varying refractive index make patterns similar to those of a quantum well with the respective potential.

The intermode trace phenomenon can be extended to other areas of wave physics. Its existence does not depend on exact form or order of the wave equations; the linearity though is required to produce eigenmodes. One can relate well known wave phenomena such as the so called Kikuchi lines in x-ray diffraction in crystals [19], Chladhi patterns in acoustics, and the formation of straight patches of calm surface in rough seas, to intermode traces. In more general terms, even nonlinear wave equations, such as, e.g., nonlinear Schrödinger, Kordeweg–De Vries, and sine-Gordon, can support multisoliton solutions, with the individual soliton trajectories reminiscent of intermode traces. The straight multisolitons traces are, e.g., found [18(d)] in the modified Kordeweg–De Vries equation approximating the propagation of EM bubbles [18(c),18(d)]. Highly organized two-dimensional nonlinear-optical patterns are formed both in the near- and far-field areas by the grid of spatial dark solitons [20], in a resonator filled with a Kerr-like nonlinear material [21], and by ''scars'' in a quantum billiard [22]. Similarly to intermode traces, these wave phenomena might be viewed as multiwave effects resulting in well-organized ''carpet'' macrostructures in systems with a broad-spectrum excitation.

In conclusion, we found characteristic highly-regular patterns in the quantum probability of multistate excitation in anharmonic potentials. They can readily be generalized to classical multimode EM field intensity distribution. We showed that these patterns can be explained and quantitatively analyzed in terms of the notion of intermode traces and their properties.

ACKNOWLEDGMENTS

We thank M. Berry, B. Ya. Zeldovich, M. Fontenelle, P. Stifter, K.A.H. van Leeuwen, N. Imoto, and A. Zeilinger for discussions. Two of us (A.E.K. and W.E.L.) thank the Humboldt Foundation for its support. The work by A.E.K. and W.P.S. was also supported by AFOSR and DFG, respectively.

[1] T. C. Weinacht, J. Ahn, and P. H. Bucksbaum, Phys. Rev. Lett. **80**, 5508 (1998); Xin Chen and J. A. Yeazell, Phys. Rev. A **56**, 2316 (1997); G. M. Lankhuijzen and L. D. Noordam, Phys. Rev. Lett. **76**, 1784 (1996); M. W. Noel and C. R. Stroud, Jr., *ibid.* **75**, 1252 (1995); **77**, 1913 (1996); L. Marmet, H. Held, G. Raithel, J. A. Yeazell, and H. Walther, *ibid.* **72**, 3779 (1994); I. Bialynicki-Birula, M. Kalinsky, and J. H. Eberly, *ibid.* **73**, 1777 (1994); M. Kalinsky and J. H. Eberly, *ibid.* **77**, 2420 (1996).

[2] G. Raithel, G. Birkl, W. D. Phillips, and S. L. Ralston, Phys. Rev. Lett. **78**, 2928 (1997).

[3] D. M. Meekhof, C. Monroe, B. E. King, W. M. Itano, and D. J. Wineland, Phys. Rev. Lett. **76**, 1796 (1996).

[4] M. Gruebele and A. Zewail, Phys. Today **43**, 24 (1990); A. Zewail, *Femtochemistry* (World Scientific, Singapore, 1994), Vols. 1 and 2; U. Leonhardt and M. G. Raymer, Phys. Rev.

Lett. **76**, 1985 (1996); T. J. Dunn, I. A. Walmsley, and S. Mukamel, *ibid.* **74**, 884 (1995); M. Shapiro, Chem. Phys. Lett. **242**, 548 (1995).

[5] F. Steininger, A. Knorr, T. Stroucken, P. Thomas, and S. W. Koch, Phys. Rev. Lett. **77**, 550 (1996).

[6] J. H. Eberly, N. B. Narozhny, and J. J. Sanchez-Mondragon, Phys. Rev. Lett. **44**, 1323 (1980); I. Sh. Averbukh and N. F. Perelman, Phys. Lett. A **139**, 449 (1989); C. Leichtle, I. Sh. Averbukh, and W. P. Schleich, Phys. Rev. Lett. **77**, 3999 (1996).

[7] (a) C. Kurtsiefer, T. Pfau, and J. Mlynek, Nature (London) **386**, 150 (1997); (b) S. Nowak, Ch. Kurtsiefer, T. Pfau, and C. David, Opt. Lett. **22**, 1430 (1996).

[8] P. L. Shkolnikov, A. E. Kaplan, and S. F. Straub, Phys. Rev. A **59**, 490 (1999).

[9] W. Kinzel, Phys. Bl. **51**, 1190 (1995).

[10] (a) M. Berry, J. Phys. A **29**, 6617 (1996); (b) M. Berry and S. Klein, J. Mod. Opt. **43**, 2139 (1996).

[11] (a) F. Grossmann, J. M. Rost, and W. P. Schleich, J. Phys. A **30**, L277 (1997); (b) P. Stifter, C. Leichtle, W. P. Schleich, and J. Marklof, Z. Naturforsch., A: Phys. Sci. **52**, 377 (1997).

[12] E. M. Wright, T. Wong, M. J. Collett, S. M. Tang, and D. F. Walls, Phys. Rev. A **56**, 591 (1997).

[13] P. Rozmej and R. Arvieu, Phys. Rev. A **58**, 4314 (1998).

[14] H. F. Talbot, Philos. Mag. **9**, 401 (1836). The modern theoretical aspects of the problem can be found in Ref. [10(b)]; for a recent brief review on the subject using the mode approach we refer to M. Mansuripur, Opt. Photonics News **8**, 43 (1997), and for a review on the temporal quantum analogy of Talbot effect, to F. Mitschke and U. Morgner, *ibid.* **9**, 45 (1998).

[15] A. E. Kaplan, P. Stifter, K. A. H. van Leeuwen, W. E. Lamb, Jr., and W. P. Schleich, Phys. Scr. **T76**, 93 (1998); see also I. Marzoli, F. Saif, I. Bialynicki-Birula, O. M. Friesch, A. E. Kaplan, and W. P. Schleich, Acta Phys. Slov. **48**, 1 (1998).

[16] See, e.g., D. Bohm, *Quantum Theory* (Prentice-Hall, Englewood Cliffs, NJ, 1951).

[17] R. L. Liboff, Int. J. Theor. Phys. **8**, 185 (1979); M. M. Nieto and L. M. Simmons, Jr., Am. J. Phys. **47**, 643 (1979).

[18] (a) A. E. Kaplan, Phys. Rev. Lett. **73**, 1243 (1994); (b) A. V. Sokolov, D. D. Yavuz, and S. E. Harris, Opt. Lett. **24**, 557 (1999); (c) A. E. Kaplan and P. L. Shkolnikov, *ibid.* **75**, 2316 (1995); (d) A. E. Kaplan, S. F. Straub, and P. L. Shkolnikov, *ibid.* **22**, 405 (1997); also in J. Opt. Soc. Am. B **14**, 3013 (1997); (e) P. B. Corkum, N. H. Burnett, and M. Y. Ivanov, Opt. Lett. **19**, 1870 (1994).

[19] S. Kikuchi, Jpn. J. Phys. **5**, 83 (1928).

[20] G. A. Swartzlander, D. R. Andersen, J. J. Regan, H. Yin, and A. E. Kaplan, Phys. Rev. Lett. **66**, 1583 (1991).

[21] S. A. Akhmanov, M. A. Vorontsov, and V. Yu. Ivanov, Pis'ma Zh. Eksp. Teor. Fiz. **47**, 611 (1988) [JETP Lett. **47**, 707 (1988)]; W. J. Firth, J. Mod. Opt. **37**, 151 (1990); F. T. Arecchi, G. Giacomelli, P. L. Ramazza, and S. Residori, Phys. Rev. Lett. **65**, 2531 (1990); G. D'Alessandro and W. J. Firth, *ibid.* **66**, 2597 (1991); L. A. Lugiato, Chaos, Solitons and Fractals **4**, 1251 (1994); S. Residori, P. L. Ramazza, E. Pampaloni, S. Boccaletti, and F. T. Arecchi, Phys. Rev. Lett. **76**, 1063 (1996).

[22] E. Heller, Phys. Rev. Lett. **53**, 1515 (1984); P. B. Wilkinson, T. M. Frombold, L. Eaves, F. W. Sheard, N. Miura, and T. Takamasu, Nature (London) **380**, 606 (1996).